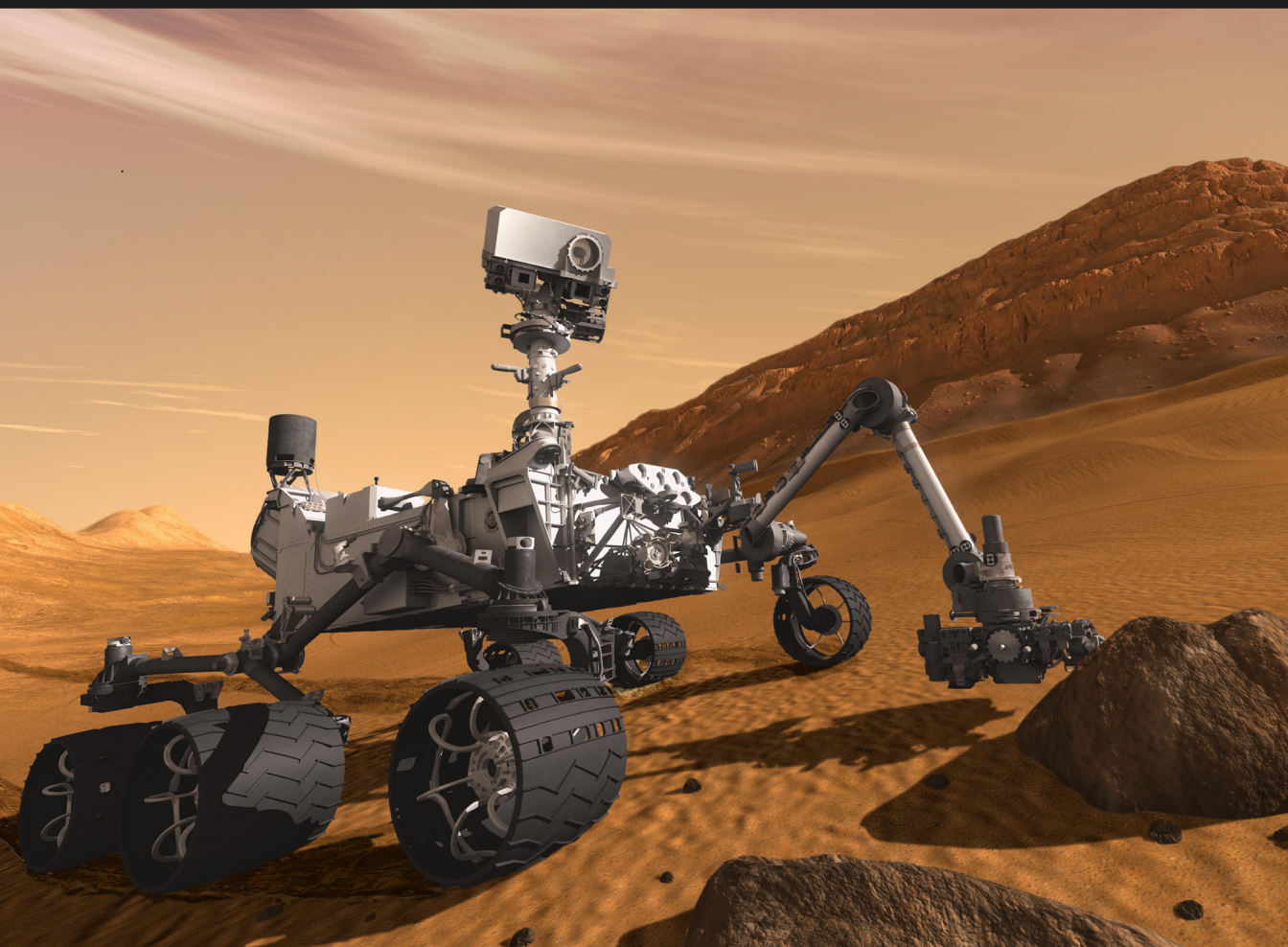


C.R. Kitchin

Remote and Robotic Investigations of the Solar System



CRC Press
Taylor & Francis Group

Remote and Robotic Investigations of the Solar System



Taylor & Francis

Taylor & Francis Group

<http://taylorandfrancis.com>

Remote and Robotic Investigations of the Solar System

By
C. R. Kitchin



CRC Press

Taylor & Francis Group

Boca Raton London New York

CRC Press is an imprint of the
Taylor & Francis Group, an **informa** business

CRC Press
Taylor & Francis Group
6000 Broken Sound Parkway NW, Suite 300
Boca Raton, FL 33487-2742

© 2018 by Taylor & Francis Group, LLC
CRC Press is an imprint of Taylor & Francis Group, an Informa business

No claim to original U.S. Government works

Printed on acid-free paper

International Standard Book Number-13: 978-1-4987-0493-9 (Hardback)

This book contains information obtained from authentic and highly regarded sources. Reasonable efforts have been made to publish reliable data and information, but the author and publisher cannot assume responsibility for the validity of all materials or the consequences of their use. The authors and publishers have attempted to trace the copyright holders of all material reproduced in this publication and apologize to copyright holders if permission to publish in this form has not been obtained. If any copyright material has not been acknowledged please write and let us know so we may rectify in any future reprint.

Except as permitted under U.S. Copyright Law, no part of this book may be reprinted, reproduced, transmitted, or utilized in any form by any electronic, mechanical, or other means, now known or hereafter invented, including photocopying, microfilming, and recording, or in any information storage or retrieval system, without written permission from the publishers.

For permission to photocopy or use material electronically from this work, please access www.copyright.com (<http://www.copyright.com/>) or contact the Copyright Clearance Center, Inc. (CCC), 222 Rosewood Drive, Danvers, MA 01923, 978-750-8400. CCC is a not-for-profit organization that provides licenses and registration for a variety of users. For organizations that have been granted a photocopy license by the CCC, a separate system of payment has been arranged.

Trademark Notice: Product or corporate names may be trademarks or registered trademarks, and are used only for identification and explanation without intent to infringe.

Front cover image: Curiosity on the surface of Mars – Artist's impression (reproduced courtesy of NASA/JPL).

Library of Congress Cataloging-in-Publication Data

Names: Kitchin, C. R. (Christopher R.), author.
Title: Remote and robotic investigations of the solar system / Chris Kitchin.
Description: Boca Raton, FL : CRC Press, Taylor & Francis Group, [2017] |
Includes bibliographical references and index.
Identifiers: LCCN 2017009368 | ISBN 9781498704939 (hardback) | ISBN 149870493X
(hardback) | ISBN 9781498704946 (e-Book) | ISBN 1498704948 (e-Book)
Subjects: LCSH: Solar system--Observations. | Astronomical instruments.
Classification: LCC QB501 .K62 2017 | DDC 629.43/5--dc23
LC record available at <https://lccn.loc.gov/2017009368>

Visit the Taylor & Francis Web site at
<http://www.taylorandfrancis.com>

and the CRC Press Web site at
<http://www.crcpress.com>

*For Rowan, Lottie, Arthur and Bob, and in loving memory of
Pip, Badger, Jess, Wills, Spruce, Misty, Chalky, Midnight, Sheba,
TC, Satchmo, Monty, Snuffles, Merlin and Bassett.*



Taylor & Francis

Taylor & Francis Group

<http://taylorandfrancis.com>

Contents

Preface, xiii

**PART I The Detection and Investigation of Solar System
Objects via Electromagnetic Radiation**

CHAPTER 1 ■ The Extended Optical Region	3
1.1 INTRODUCTION	3
1.2 TELESCOPES AND CAMERAS	7
1.2.1 Reflecting Cameras	7
1.2.1.1 Prime Focus Systems	10
1.2.1.2 Cassegrain Systems	10
1.2.1.3 Ritchey–Chrétien Systems	11
1.2.1.4 Catadioptric Systems	13
1.2.1.5 Gregorian Systems	17
1.2.1.6 Custom-Designed Systems	17
1.2.2 Refracting Cameras	20
1.2.2.1 Telescope-Type Systems	20
1.2.2.2 Camera-Type Systems	21
1.2.2.3 Panoramic Systems	24
1.3 SPECTROSCOPY AND SPECTROGRAPHS	26
1.3.1 Introduction	26
1.3.2 Basic Spectroscopy	26
1.3.3 Spectrographs	38
1.3.4 Spectral Features	38
1.3.5 Examples of Spectrographic Instruments	41
1.4 DETECTORS	49
1.4.1 Electron–Hole Pair Production-Based Detectors	49
1.4.1.1 Introduction	49

1.4.1.2	CCDs	50
1.4.1.3	<i>Complementary Metal-Oxide Semiconductor Detectors</i>	54
1.4.1.4	<i>Photodiodes</i>	54
1.4.2	Thermal Detectors	55
1.4.3	Photoelectric Effect-Based Detectors	56
1.4.3.1	<i>Introduction</i>	56
1.4.3.2	<i>Microchannel Plates</i>	56
1.4.3.3	<i>Photomultipliers</i>	57
1.4.3.4	<i>Image Intensifiers</i>	58
1.4.3.5	<i>Detectors of Historical Interest</i>	58
CHAPTER 2 ■ Microwave and Radio Regions		61
2.1	INTRODUCTION	61
2.2	TELESCOPES, RECEIVERS AND DETECTORS	63
2.3	DIRECT EMISSIONS FROM SOLAR SYSTEM OBJECTS	67
2.3.1	Introduction	67
2.3.2	Space-Based Observations	70
2.4	RADAR	72
2.4.1	Introduction	72
2.4.2	Physical Principles of Radar Systems	73
2.4.3	Terrestrially Based Instruments	74
2.4.4	Spacecraft-Based Instruments	79
2.4.4.1	<i>Introduction</i>	79
2.4.4.2	<i>Synthetic Aperture Radar</i>	79
2.4.4.3	<i>Imaging Radar Spacecraft Missions</i>	83
2.4.4.4	<i>Altitude, Doppler, Terrain and Other Radars</i>	84
2.4.4.5	<i>Ground-Penetrating Radar</i>	87
2.4.4.6	<i>Occultations</i>	88
2.5	SPECTROSCOPY	90
CHAPTER 3 ■ X-Ray and γ Ray Regions		95
3.1	INTRODUCTION	95
3.1.1	Early Observations	96
3.1.1.1	<i>X-Rays</i>	96
3.1.1.2	<i>Gamma Rays</i>	96
3.1.2	X- and γ Ray Sources	97

3.2	DETECTORS	99
3.2.1	Introduction	99
3.2.2	Proportional Counters and Related Instruments	99
3.2.3	Scintillation Detectors	103
3.2.4	Microchannel Plates and Related Instruments	105
3.2.5	Solid State Detectors and Related Instruments	106
	3.2.5.1 <i>Charge-Coupled Devices</i>	107
	3.2.5.2 <i>Semiconductor-Based Detectors</i>	114
	3.2.5.3 <i>Calorimeter</i>	116
3.3	IMAGERS	117
3.3.1	Multi-Layer Reflectors	118
3.3.2	Glancing Incidence Reflectors	118
	3.3.2.1 <i>Macroscopic Systems</i>	119
	3.3.2.2 <i>Microscopic Systems</i>	122
3.3.3	Collimators	126
	3.3.3.1 <i>Pin-Hole Cameras</i>	126
	3.3.3.2 <i>Honeycomb Collimators</i>	127
3.3.4	Coded Masks	128
3.4	SPECTROSCOPES	131
3.4.1	Grating-Based Spectroscopes	132
	3.4.1.1 <i>Transmission Gratings</i>	132
	3.4.1.2 <i>Reflection Gratings</i>	132
3.4.2	Bragg Diffraction-Based Spectrometers	133
PART II	The Detection and Investigation of Sub-Atomic, Atomic and Molecular Particles	
CHAPTER 4	■ Detectors	139
<hr/>		
4.1	INTRODUCTION	139
4.2	DETECTORS	140
4.2.1	Geiger Counters	141
4.2.2	Ion Chambers	145
4.2.3	Proportional Counters	147
4.2.4	Scintillation Detectors	148
4.2.5	Microchannel Plates	151
	4.2.5.1 <i>Channel Electron Multiplier</i>	155

4.2.6	Solid State Detectors	156
4.2.6.1	<i>Semiconductors and the Band Structure of Solids</i>	156
4.2.6.2	<i>Solid State Detectors</i>	160
4.2.7	Transition Radiation Detectors	163
4.2.8	Calorimeter	165
4.2.9	Čerenkov Detectors	165
CHAPTER 5 ■ Ion Optics and Charged Particle Instrumentation		169
5.1	INTRODUCTION	169
5.2	ION OPTICS AND CHARGED PARTICLE INSTRUMENTATION	169
5.2.1	Electrostatic Analyser	169
5.2.2	Electrostatic Lenses	176
5.2.3	Electrostatic Prisms	177
5.2.3.1	<i>Quadrupole Beam Deflector</i>	177
5.2.4	Magnetic Interactions	177
5.2.4.1	<i>Introduction</i>	177
5.2.4.2	<i>Magnetic Lenses</i>	179
5.2.5	Velocity Selectors and Spectrometers	182
5.2.5.1	<i>Velocity Selector</i>	182
5.2.5.2	<i>Velocity Spectrometer</i>	182
5.2.5.3	<i>Ion Drift Meters</i>	183
5.2.6	Mass Spectrometers	184
5.2.6.1	<i>Introduction</i>	184
5.2.6.2	<i>Magnetic Sector Mass Spectrometer</i>	184
5.2.6.3	<i>Electric Fields</i>	188
5.2.6.4	<i>Time-of-Flight Mass Spectrometer</i>	191
5.2.6.5	<i>Future Usage of Mass Spectrometers</i>	194
CHAPTER 6 ■ Neutral Particles		195
6.1	INTRODUCTION	195
6.2	NEUTRON DETECTION	196
PART III Direct Sampling and Other Investigative Methods		
CHAPTER 7 ■ Direct Sampling Instruments		203
7.1	INTRODUCTION	203
7.2	SURFACE	206

7.2.1	Microscopy	207
7.2.2	Spectroscopy	209
7.2.2.1	<i>Thermal Emissions</i>	209
7.2.2.2	<i>Solids</i>	210
7.2.2.3	<i>Gases</i>	212
7.2.2.4	<i>Raman Spectroscopy</i>	212
7.2.2.5	<i>X-Ray Fluorescence Spectroscopy and X-Ray Diffraction</i>	214
7.2.2.6	<i>Alpha Particle Spectrometry</i>	216
7.2.2.7	<i>Mössbauer Spectroscopy</i>	218
7.2.3	Chemical and Biological Analyses	219
7.2.3.1	<i>Introduction</i>	219
7.2.3.2	<i>Gas Chromatograph</i>	219
7.2.3.3	<i>Gas Chromatograph–Mass Spectrometer Instruments</i>	220
7.2.3.4	<i>Biological Investigations</i>	223
7.2.3.5	<i>Neutron-Based Instruments</i>	224
7.2.3.6	<i>Wet Chemistry</i>	226
7.2.4	Physical Properties	227
7.2.4.1	<i>Temperature and Thermal Conductivity or Inertia</i>	227
7.2.4.2	<i>Electricity and Magnetism</i>	229
7.2.4.3	<i>Density and Refractive Index</i>	231
7.2.5	Ionising Radiation Levels	232
7.2.6	Sampling	233
7.2.6.1	<i>Introduction</i>	233
7.2.6.2	<i>Passive Sampling</i>	234
7.2.6.3	<i>Active Sampling</i>	234
7.2.7	Ground Truth	242
7.2.8	Retro-Reflectors	243
7.3	SUB-SURFACE	244
7.3.1	Radar	244
7.3.2	Seismometry	245
7.3.2.1	<i>Introduction</i>	245
7.3.2.2	<i>Spacecraft Seismometry</i>	247
7.4	ATMOSPHERE	248
7.4.1	Spectroscopy	248
7.4.2	Nephelometry	250

7.4.3	Pressure	250
7.4.4	Temperature	252
7.4.5	Humidity	253
7.4.6	Wind	254
7.4.7	Acoustics	255
7.5	INTERPLANETARY MEDIUM	255
7.5.1	Large-Scale Magnetic Fields	256
7.5.1.1	<i>Search Coil Magnetometer</i>	256
7.5.1.2	<i>Flux Gate Magnetometer</i>	257
7.5.1.3	<i>Helium Magnetometer</i>	259
7.5.2	Electric Fields	259
7.5.2.1	<i>Langmuir Wave Instruments</i>	259
7.5.2.2	<i>Langmuir Probe Instruments</i>	261
7.5.2.3	<i>Electron Drift</i>	263
7.5.3	Interplanetary Dust	263
CHAPTER 8	■ Accelerations	267
8.1	INTRODUCTION	267
8.2	SPACECRAFT-BORNE ACCELEROMETERS	268
8.3	GRAVITY STUDIES	269
APPENDIX A:	BIBLIOGRAPHY	273
APPENDIX B:	TIMELINE OF SOLAR SYSTEM INVESTIGATIONS	279
APPENDIX C:	DETAILS OF THE SPACECRAFT, ROCKETS, OBSERVATORIES AND OTHER MISSIONS MENTIONED IN THIS BOOK	295
APPENDIX D:	DATA AND UNITS	331
APPENDIX E:	ABBREVIATIONS AND ACRONYMS	337
INDEX		347

Preface

The purpose of this book is to explain how our present knowledge of solar system objects, other than the Sun, has been obtained. We are thus concerned with investigations of planets, dwarf planets, asteroids, natural satellites, comets, Kuiper belt objects and the interplanetary medium. The book examines the instruments used to obtain observations, samples, measurements, analyses, etc., of the interiors, surfaces, atmospheres and radiation belts of these solar system objects. It describes the underlying physical principles of the instruments and the way in which these principles have been used to design actual instruments. It is not about the results of those investigations (except occasionally in passing). There are plenty of excellent sources describing what our current knowledge of solar system objects is, but detailed and comprehensive descriptions of the basic methods used to obtain that knowledge are far more difficult to find. This book aims to remedy that situation by gathering all that data together in one easily accessible place, linking descriptions of the physical principles to the design of working instruments and illustrating both with examples of real instruments in use.

The bulk of the book concentrates on the period from the launch of Sputnik 1 (4 October 1957) to the present day and looks forward to possible future developments. The majority of instruments discussed are spacecraft borne, but instruments on rockets, balloons and terrestrial telescopes are also included. Appendix B gives a timeline covering more than 4000 years of observations and theoretical ideas about the solar system for readers who would like to set the modern developments into a historical perspective.

Well over 250 individual spacecraft, rockets, balloons, terrestrial instruments and observatories are mentioned in this book when discussing individual examples. Rather than repeat definitions and details (such as launch dates, objectives, orbits, operator, etc.) every time a particular mission is mentioned, these details are listed in Appendix C along with those of their instruments discussed herein. The number of Earth observation spacecraft is large,* so only a small selection of them has been chosen for discussion, otherwise they would overwhelm the missions to other solar system objects.

Abbreviations and acronyms are defined the first time they are used in the text and then listed alphabetically for convenience in Appendix E. Appendix D lists some definitions and values of physical constants and laws used in the book.

* At the start of 2017, for example, India launched 103 Earth-orbiting spacecraft from a single rocket.

This book has the same approach to solar system instrumentation as the author's book *Astrophysical Techniques* (Appendix A, reference A.1.1) regarding the instrumentation used to observe the wider universe. This book, however, is intended to be a stand-alone work and so some material is covered in both books. Generally, the level of treatment when the same topics are covered will be different because terrestrial-based studies play a much bigger role in investigating the wider universe and spacecraft-based instruments are generally more important within the solar system.

Readers will need to be familiar with some physics and mathematics to university entrance level for a physical sciences subject to follow some discussions. But generally, the discussions are not that demanding and many of the physical principles involved are described *ab initio* within this book.

Apart from occasional references, specialised instruments for solar observing have been omitted. This is because they are covered in the author's book *Solar Observing Techniques* (Appendix A, reference A.1.6) and because the Sun is so different in its nature from the other solar system objects that instruments developed for its study do not find many applications elsewhere.

I hope that you will find this book interesting and useful and perhaps learn a few new things from it – I have certainly done so while writing it!

C. R. Kitchin
University of Hertfordshire

I

The Detection and Investigation of Solar System Objects via Electromagnetic Radiation



Taylor & Francis

Taylor & Francis Group

<http://taylorandfrancis.com>

The Extended Optical Region

1.1 INTRODUCTION

In this first part, the aim is to describe, explain and discuss the ways in which our knowledge of the solar system and its contents has been enlarged and enhanced by remote and robotic investigations utilising the photons emitted or reflected from solar system objects. Later parts will deal with more direct and interactive investigations.

Readers of this book are likely to be familiar with the dual wave-particle nature of electromagnetic (e-m) radiation. A reminder of what this implies for the design of instrumentation, etc. however may not come amiss – thus the wave nature of light enables a telescope lens or mirror to focus a beam of (wave) radiation into an image, whilst the detector, in most cases, will utilise the particle nature of light to pick up individual photons.

When behaving as a wave, e-m radiation is described by its frequency (ν or f^*) and wavelength (λ) and, in a vacuum, the two quantities are related to the velocity of light in a vacuum (c) by

$$\lambda\nu = c \tag{1.1}$$

The e-m radiation in its particle manifestation is described by the energy of the individual photons (quanta) that are involved. The wave and particle descriptions are linked by the Planck formula

$$E = h\nu \tag{1.2}$$

where h is Planck's constant ($6.62607 \times 10^{-34} \text{ m}^2 \text{ kg s}^{-1}$) and E is the photon's energy.

Conversion between the frequency, wavelength and energy of e-m radiation is often needed and the formulae

* Definitions and, where appropriate, values of symbols and quantities are listed in Appendix D. There, where possible, the full up-to-date values are quoted together with the (generally) more approximate values used for calculations within this book.

4 ■ Remote and Robotic Investigations of the Solar System

$$\begin{aligned} \text{Frequency (Hz)} &\approx 3.00 \times 10^8 \div \text{Wavelength (m)} \\ &\approx 1.50 \times 10^{33} \times \text{Energy (J)} \\ &\approx 2.40 \times 10^{14} \times \text{Energy (eV)} \end{aligned} \quad (1.3)$$

$$\begin{aligned} \text{Wavelength (m)} &\approx 3.00 \times 10^8 \div \text{Frequency (Hz)} \\ &\approx 2.00 \times 10^{-25} \div \text{Energy (J)} \\ &\approx 1.25 \times 10^{-6} \div \text{Energy (eV)} \end{aligned} \quad (1.4)$$

$$\begin{aligned} \text{Energy (J)} &\approx 1.60 \times 10^{-19} \times \text{Energy (eV)} \\ &\approx 6.66 \times 10^{-34} \times \text{Frequency (Hz)} \\ &\approx 2.00 \times 10^{-25} \div \text{Wavelength (m)} \end{aligned} \quad (1.5)$$

$$\begin{aligned} \text{Energy (eV)} &\approx 6.24 \times 10^{-18} \times \text{Energy (J)} \\ &\approx 4.16 \times 10^{-15} \times \text{Frequency (Hz)} \\ &\approx 1.25 \times 10^{-6} \div \text{Wavelength (m)} \end{aligned} \quad (1.6)$$

may be found useful (where the quantities are in the units usually used).

The e-m spectrum thus theoretically ranges from zero frequency or energy (infinite wavelength) to infinite frequency or energy (zero wavelength). It is customarily subdivided, in terms of its frequency, into the regions:*

$$\begin{aligned} &0 \leftrightarrow \text{Extremely low frequency (ELF)} \leftrightarrow \text{Radio} \leftrightarrow \text{Microwave} \\ &\leftrightarrow \text{Far infrared (FIR}^\dagger) \leftrightarrow \text{Medium infrared (MIR)} \leftrightarrow \text{Near infrared (NIR)} \leftrightarrow \text{Visible}^\ddagger \\ &\leftrightarrow \text{Ultraviolet} \leftrightarrow \text{Soft x-rays} \leftrightarrow \text{Hard x-rays} \leftrightarrow \gamma \text{ rays} \leftrightarrow \infty \end{aligned}$$

The approximate extents of these regions are shown in Table 1.1 together with conversions between wavelength, frequency and energy for quick reference.

E-m radiation is generally, but by no means always, discussed in terms of its frequency at low energies (ELF, radio, microwave regions), by its wavelength in the intermediate region (infrared [IR], visible and ultraviolet [UV] regions) and by the photon energy in the x-ray and γ ray regions. This practice is mainly historical in origin, but remains convenient in that the numbers thus being used have relatively small powers of ten in their expressions.

A reminder may also be useful that e-m radiation interacts with matter in different ways depending upon its energy (particle character)/frequency (wave character). Thus, the main interactions are:

* There are many other ways of dividing up the e-m spectrum. The microwave region, for example, is sometimes subdivided into eight bands such as the S band (2–4 GHz) and the Ku band (12.5–18 GHz). Visible light is, of course subdivided into the colours: red, orange, yellow, . . . , violet, etc.

† Sometimes called Terahertz or sub-millimetre radiation.

‡ The NIR, visible and long-wave ultraviolet regions are often combined and referred to as the optical region.

TABLE 1.1 The Regions of the e-m Spectrum and the Interrelationships between Frequency, Wavelength and Photon Energy

	Wavelength (m)	Frequency (Hz)	Energy (eV)	Energy (J)
ELF	∞	0	0	0
	↑	↑	↑	↑
	1.00×10^5	3.00×10^3	1.24×10^{-11}	1.99×10^{-30}
Radio	↓	↓	↓	↓
	1.00	3.00×10^8	1.24×10^{-6}	1.99×10^{-25}
Microwave	↓	↓	↓	↓
	1.00×10^{-3}	3.00×10^{11}	1.24×10^{-3}	1.99×10^{-22}
FIR	↓	↓	↓	↓
	1.00×10^{-4}	3.00×10^{12}	1.24×10^{-2}	1.99×10^{-21}
MIR	↓	↓	↓	↓
	1.00×10^{-5}	3.00×10^{13}	0.124	1.99×10^{-20}
NIR	↓	↓	↓	↓
	3.80×10^{-7}	4.00×10^{14}	1.65	2.65×10^{-19}
Visible	↓	↓	↓	↓
	3.80×10^{-7}	7.89×10^{14}	3.26	5.24×10^{-19}
Ultraviolet	↓	↓	↓	↓
	1.00×10^{-8}	3.00×10^{16}	1.24×10^2	1.99×10^{-17}
Soft x-rays	↓	↓	↓	↓
	1.00×10^{-10}	3.00×10^{18}	1.24×10^4	1.99×10^{-15}
Hard x-rays	↓	↓	↓	↓
	1.00×10^{-11}	3.00×10^{19}	1.24×10^5	1.99×10^{-14}
γ rays	↓	↓	↓	↓
	0	∞	∞	∞

ELF and radio radiation – direct induction of electric currents, synchrotron and free-free emissions and absorptions

Microwave and Infrared – molecular rotational and vibrational emissions and absorptions

Optical – interactions with the outer electrons of atoms, ions and molecules

UV and x-ray – interactions with the inner electrons of atoms and ions, ionisation and recombination

X-ray and γ rays – interactions directly with nuclei

Thermal radiation can be emitted by materials at any temperature when their constituent atoms or molecules undergo changes of velocity during their interactions with other nearby atoms or molecules. The change in velocity results in bremsstrahlung* radiation. In liquids and gases, the particles are free to move around. In solids, the particles are more or less fixed in place, but vibrate about their mean positions within the material so that

* The German word for ‘braking radiation’. Both synchrotron and free-free radiation are also forms of bremsstrahlung radiation.

the individual radiation patterns have a dipole nature. Thermal radiation's spectrum* is described by the Planck equation and its emissions peak at a wavelength or frequency for a particular temperature given by Wien's displacement law.

Planck equation:

$$I(\nu, T) d\nu = \frac{2h\nu^3 \mu^2}{c^2 (e^{h\nu/kT} - 1)} \quad (1.7)$$

$$I(\lambda, T) d\lambda = \frac{2hc^2 \mu^2}{\lambda^5 (e^{hc/\lambda kT} - 1)} \quad (1.8)$$

and

$$I(\nu, T) d\nu = I(\lambda, T) d\lambda \quad (1.9)$$

where $I(\nu, T)$ and $I(\lambda, T)$ are the thermal radiation intensities at temperature T and in terms of frequency and wavelength, respectively, and μ is the refractive index of the material forming the transmission medium (equal to 1 for a vacuum).

Wien's displacement law:

$$\lambda_{\text{Max}} = \frac{2.898 \times 10^{-3}}{T} \text{ m} \quad (1.10)$$

$$\nu_{\text{Max}} = 5.879 \times 10^{10} T \text{ Hz} \quad (1.11)$$

where λ_{Max} and ν_{Max} are the wavelength and frequency of the maximum thermal emission per unit wavelength and unit frequency intervals.†

Measurements of e-m radiation can, theoretically, determine its frequency (or wavelength or photon energy), its intensity at a particular frequency (and also the variation of its intensity as the frequency changes – i.e. the spectrum), its variation in intensity in one, two or three dimensions (i.e. the direction of its sources/imaging), its state of polarization and its phase. Generally, only at low frequencies can all these properties of radiation be determined and at the highest frequencies, measurements are limited largely to determining the radiation's intensity and direction.

Particularly for the spacecraft-borne instrumentation used for studying the objects within the solar system, the main observing region of the spectrum ranges from microwaves to soft x-rays. Over much of this region instruments' operating principles are clearly related to each other, although the details vary. We shall therefore start by looking at the instrumentation used over the MIR to UV parts of the spectrum before going on to consider instruments operating at lower or higher frequencies. Since, as already mentioned, the term

* Also often called the blackbody spectrum.

† Since the wavelength unit interval is 1 m and the frequency unit interval is 1 Hz the maxima occur at different parts of the spectrum (e.g. at 1000 K, $\lambda_{\text{Max}} = 2.898 \times 10^{-6} \text{ m} (= 1.05 \times 10^{14} \text{ Hz})$, $\nu_{\text{Max}} = 5.879 \times 10^{13} \text{ Hz} (= 5.10 \times 10^{-6} \text{ m})$).

‘optical region’ is generally used for the NIR, visible and near UV regions, it is convenient to use the term ‘extended optical region’ (EOR), to include the MIR and far UV regions as well.

1.2 TELESCOPES AND CAMERAS

Most people find that the direct images of objects, whether black and white, colour or false colour, are the most vivid and impressive results from spacecraft solar system missions. The implications of such images may normally be understood immediately, without (or without much) specialist training. From a scientific point of view, images contain a wealth of information and form an invaluable reference archive even after they have been used for their primary purpose(s). Obtaining images over the EOR customarily involves using telescopes – or since the instruments do not use eyepieces, what should more properly be called cameras.

Apart from the lack of an eyepiece, the cameras on spacecraft are often identical in their designs to terrestrial telescopes, or are minor variants of such designs. Both refracting (lens-based, dioptric) and reflecting (mirror-based, catoptric) instruments are in use, with the latter being the more common. There are also some custom-built optical systems that have been designed (usually) because of constraints on mass or size required within a particular spacecraft.

Almost all of these camera designs may include additional optics to fold the light beam in order to shorten the instrument’s length or to direct the image to a convenient place. Most cameras have interchangeable filters to enable images to be obtained within different parts of the spectrum and/or be multipurpose instruments obtaining direct images or spectra (Section 1.3) or both simultaneously.

The reader is assumed to be familiar with the basics of the optics of light – laws such as those of reflection and refraction and terms such as focal plane, field of view, focal length, focal ratio, etc. The basic principles of usual designs of cameras (telescopes) are likely to be familiar to most readers of this book, but if not, Appendix A lists various sources suitable for background reading. Here just a brief summary of the main designs is given with examples of their use in actual missions.

1.2.1 Reflecting Cameras

Some cameras are based just upon a single concave parabolic mirror with the detector or detector array placed at its focus – a system known as a prime focus instrument when used for terrestrial telescopes (Figure 1.1a). Subsidiary lenses or mirrors will generally be needed to correct the aberrations* inherent in a simple parabolic mirror, providing a wider, sharply focussed, field of view. The Cassegrain design (Figure 1.1b) uses a concave parabolic primary mirror and a convex hyperbolic secondary mirror. The closely related Ritchey–Chrétien instruments have a wider field of sharp focus than a similar Cassegrain and use a concave hyperbolic primary mirror and a convex hyperbolic secondary mirror. Some Gregorian-based designs (Figure 1.1c) are also to be encountered with a concave elliptical secondary mirror placed after the primary focus.

* See reference A.1.1 for a detailed discussion of the Seidel aberrations of optical systems, or other sources listed in Appendix A.

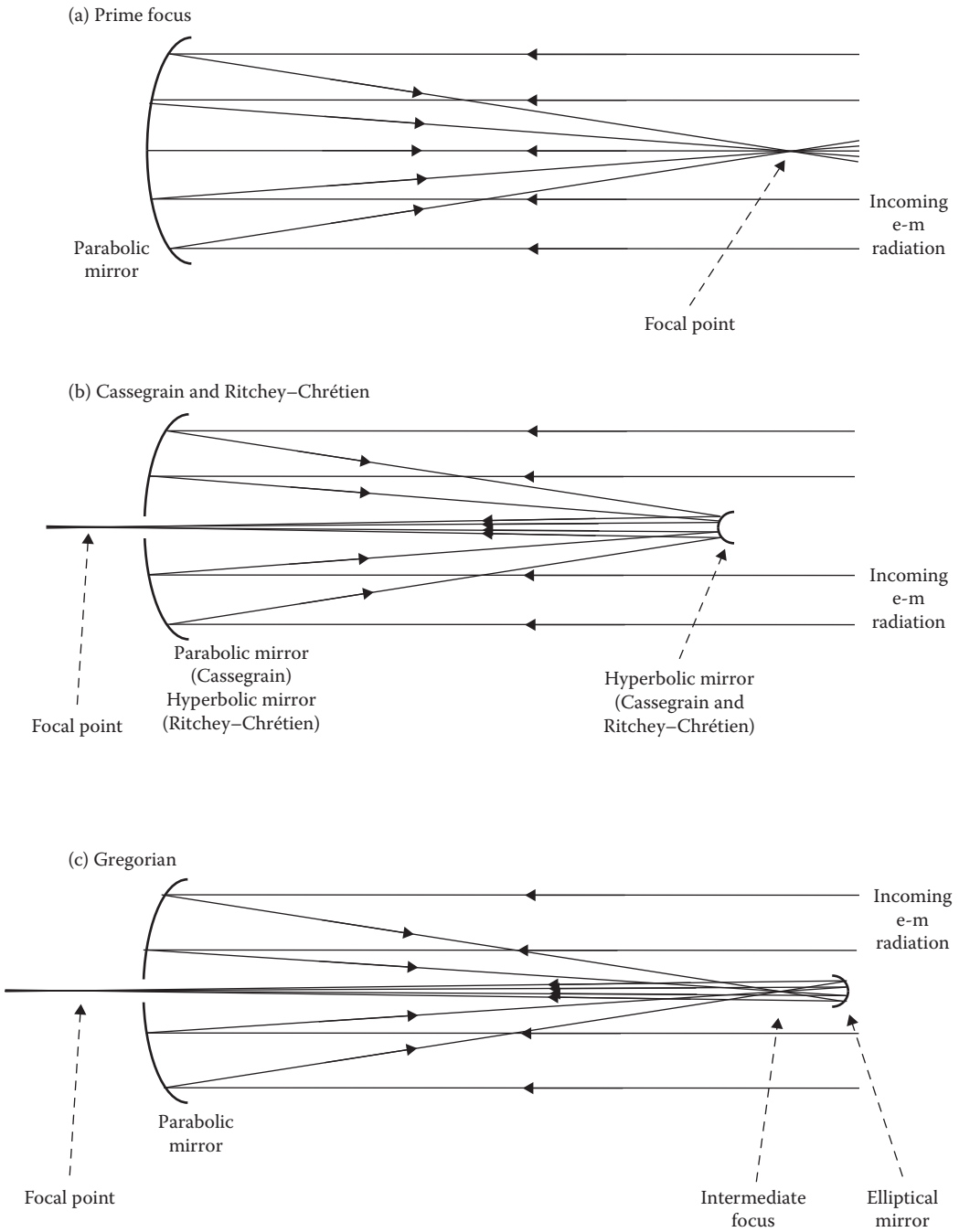


FIGURE 1.1 Light paths in the main camera designs: (a) prime focus, (b) Cassegrain and Ritchey-Chrétien, and (c) Gregorian.

(Continued)

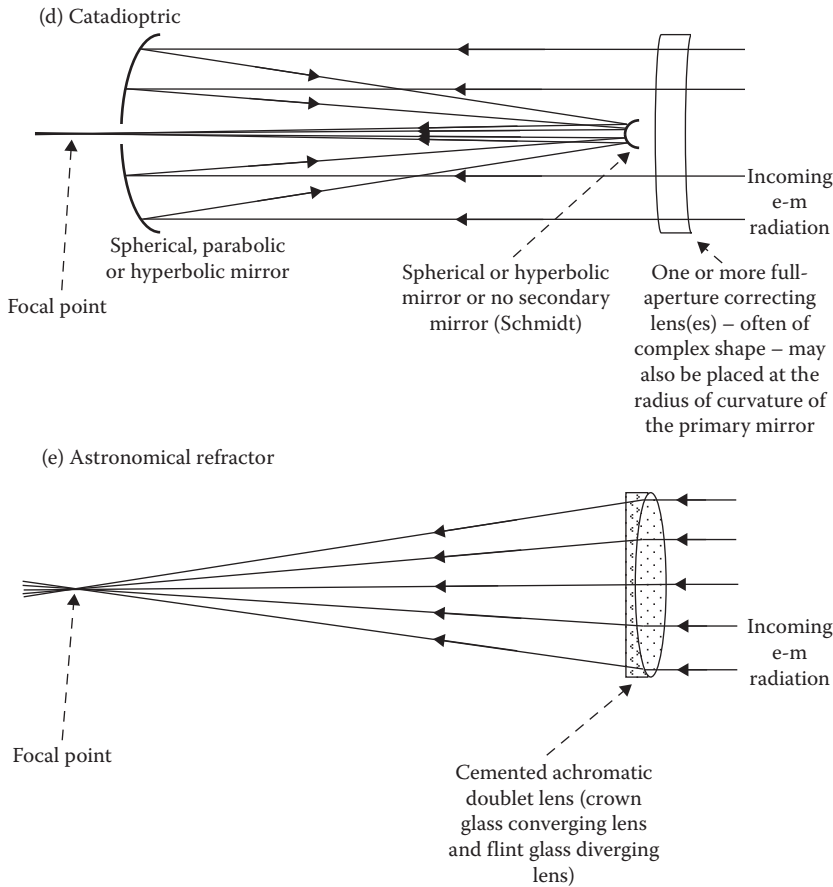


FIGURE 1.1 (Continued) Light paths in the main camera designs: (d) Catadioptric and (e) Astronomical refractor.

Catadioptric instruments, such as the Schmidt camera and the very popular commercially produced compact Schmidt–Cassegrains aimed at the amateur astronomy market, use both mirrors and lenses as their primary radiation-gathering elements (Figure 1.1d). The Schmidt design has a spherical primary mirror and an aspherical correcting lens placed at its radius of curvature and provides a very large field of view. The original Schmidt–Cassegrain design uses a spherical primary, an aspherical correcting lens and a spherical secondary mirror. In the compact Schmidt–Cassegrain, the correcting lens is placed at or just inside the primary mirror’s focal point, thus halving the tube length. The primary and secondary mirrors may be spherical, parabolic or hyperbolic – there are many variations. The Makzutov design is very similar to the compact Schmidt–Cassegrain but uses a spherical primary mirror and a meniscus correction lens with both surfaces spherical, and has the secondary mirror aluminized at the centre of the correcting lens on its inner

surface – the secondary mirror is therefore also spherical. Examples of some of these designs, mostly small, may occasionally be used within instruments on board spacecraft.

A number of individual cameras that have been used or are being used for solar system investigations are discussed below to illustrate the range of the possibilities. Detector types which operate within the EOR and their theory and practice are covered in Section 1.4. They are mentioned however here, as well, in order to complete the instrument' descriptions.

1.2.1.1 Prime Focus Systems

Mars Atmosphere and Volatile Evolution Mission (MAVEN)* is a Mars orbiter launched in November 2013 by the National Aeronautics and Space Administration (NASA) and still operating at the time of writing. Its Imaging Ultraviolet Spectrometer (IUVS), although principally functioning as a spectrograph (Section 1.3), has a direct imaging mode as well. The spherical primary mirror has a 13.3 mm × 20 mm aperture and a 100 mm focal length. The spectrograph entrance slit is at the prime focus of the primary mirror. The primary mirror is fed by a plane scanning mirror and can point towards the Martian limb with a field of view of 12.5° × 24° or towards the Martian surface below the spacecraft (nadir) with a field of view of 12.5° × 60°. The spectrograph's entrance slit measures 0.06° × 212.5°. IUVS observes over the 110–340 nm spectral region using two detectors. A beam splitter separates the radiation into two beams, one covering the 110–180 nm region, the other the 180–320 nm region. The detectors are 1024 × 1024 CMOS† arrays that are fed by image intensifiers. The image intensifiers use UV optimised photocathodes – caesium telluride for the longer wavelengths and caesium iodide for the shorter wavelengths.

Direct imaging is accomplished through the nadir field of view when the spacecraft is near apareon (the highest point in its orbit – about 6000 km above the Martian surface). The scanning mirror sweeps the field of view seen through the spectrograph slit over a swath of the surface to build up an image at a particular UV wavelength with a surface resolution of ~160 km (cf. pushbroom scanning, Section 1.2.1.3).

1.2.1.2 Cassegrain Systems

The two Japan Aerospace Exploration Agency (JAXA) asteroid sample-return spacecraft, Hayabusa 1 and 2, use Cassegrain-design cameras for their LIDAR‡ systems. The LIDAR is used to measure the distance of the spacecraft from its target over the range ~30 m to ~25 km and for surface and topographical measurements of the asteroid. The silicon-carbide primary mirrors have 127 mm diameters and focal ratios of about 1.5. The laser uses a 17 W neodymium-doped yttrium aluminium garnet (Nd:YAG) crystal with a pulse length of 14 ns operating at 1064 nm. Detection of the returned pulse is by a silicon avalanche photodiode (APD – Section 1.4.1.4). The Cassegrain optics are used for the range 1–25 km. A separate small receiver is used for the 30 m to 1 km range.

* Acronyms and abbreviations are listed within the text when first introduced and also listed alphabetically in Appendix E. Details of spacecraft and their instrumentation described in this book are listed in Appendix C.

† Complementary metal-oxide semiconductor – see Section 1.4.1.3.

‡ Light detection and ranging (cf. RADAR – Section 2.4).

The lunar mapper, Clementine, carried several imagers (see also Section 1.2.2.2). Its $f/2.67$ Long Wave Infrared Camera (LWIC) was of the Cassegrain design with a 131 mm diameter primary mirror and relay lenses. With a 1° field of view and a 128×128 pixel HgCdTe detector (Sections 1.4.1.1 and 1.4.1.4) its surface resolution on the Moon was ~ 50 m at best. It operated over the $8.0\text{--}9.5$ μm spectral region.

The Earth imaging Deep Space Climate Observatory (DSCOVR) observes Earth from the L1* point using a 300 mm Cassegrain telescope (EPIC – Earth Polychromatic Imaging Camera). It has 10 narrow band (1–3 nm) filters distributed over the 317–780 nm spectral range and uses a 2048×2048 pixel charge-coupled device (CCD) (Section 1.2.1.2) array as its detector.

A spacecraft originally built for surveying infrared galaxies was later repurposed into discovering near-Earth asteroids. The remarkable transformation happened to the Wide field Infrared Survey Explorer (WISE) spacecraft which, for its new mission, was named Near Earth Object Wide field Infrared Survey Explorer (NEOWISE). Its telescope is a 400 mm Cassegrain with a gold coating. Its field of view is $47'$ across and its angular resolution $5''$. A further 13 mirrors follow the main telescope. All the mirrors are diamond turned aluminium with gold coatings. Until its coolant ran out, the optics were cooled to 17 K. A beam splitter separates the incoming light into four channels centred on 3.4, 4.6, 12 and 22 μm and two cameras each accept two of the channels for imaging. The first two channels use a 1024×1024 pixel HgCdTe array (Sections 1.4.1.1 and 1.4.1.4) and the second two channels use a SiAs blocked impurity band (BIB) array (Section 1.4.1.4) of the same size. A scan mirror counteracts the spacecraft's rotation during each 8.8-second exposure. WISE imaged some 750 million objects (including many asteroids), while NEOWISE has since discovered ~ 250 near-Earth asteroids and two possible comets.

The aircraft-borne $f/1.3$, 2.5 m SOFIA (Stratospheric Observatory for Infrared Astronomy) is also a Cassegrain-type instrument with a third 45° flat mirror to reflect its light beam to a Nasmyth† focus. It can operate from 300 nm to 655 μm wavelengths using a variety of instruments. Two weeks before New Horizon's fly-by of Pluto it was able to observe an occultation by Pluto with its high speed photometer revealing the structure of Pluto's atmosphere. It has also been used to detect atomic oxygen in the atmosphere of Mars and to map Jupiter in the FIR.

1.2.1.3 Ritchey–Chrétien Systems

The comet probe, Giotto, sent by the European Space Agency (ESA) to fly by Halley's comet in March 1986 carried the Halley Multicolor Camera (HMC). This instrument had Ritchey–Chrétien optics with a 160 mm aperture and 1 m effective focal length. The camera was mounted within the spacecraft body for protection and viewed the comet via a plane

* The Lagrange points (L1, L2, L3, L4 and L5) are points in space where a small object can maintain a stable position with respect to much larger bodies that are orbiting each other. The L1, L2 and L3 point lie along the line joining the two main bodies, with L1 between the two main bodies and L2 and L3 outside them. L4 and L5 share the same orbit as the smaller of the two main bodies and lie 60° ahead and 60° behind that body. The Trojan and Greek asteroids occupy the L5 and L4 points, respectively, for several planets, especially Jupiter.

† A third, plane, mirror set at 45° sends the light beam of the telescope through a hollow altitude axis of the telescope's Alt-Az mounting to a focus whose position is fixed whatever altitude the telescope may point to (cf. Coudé focus for equatorially mounted telescopes).

45° mirror which was the only part of the instrument directly exposed to impacts by dust particles.* The instrument had a field of view of 1.5° and could be moved through 180° in a plane that was parallel to the spacecraft's spin axis. The spin, at 15 rpm, then allowed the HMC to image any part of the sky – an observing method known as pushbroom scanning.

Two 390 × 584 pixel CCDs (see Section 1.4.1.2) were used as the detectors and divided into two sections each. One of the sections was clear, two had fixed filters – one red and one blue. The final section imaged through a filter wheel containing 11 filters and polarisers. The image was split using two mirrors set at 90° to each other, placed just before the focal plane and which reflected the light beam out to the sides and onto the two CCDs. The images from each of the CCD sections were thus of slightly different parts of the comet. A 2 × 936 pixel Reticon™ silicon photodiode detector (Section 1.4.1.4) placed to the side of the mirrors received the image directly and was used for pointing the camera towards the comet.

Light entered the CCD detector sections through narrow slits so that only a line of the CCD section, some four to eight pixels wide, was illuminated at any given instant. The spacecraft's rotation moved the illuminated line across the CCD and the accumulating electric charges within the detector array were moved to keep pace with it (time-delayed integration – TDI – see Section 1.4.1.2). The resolution at the comet's nucleus was 10 m from a distance of 500 km.

The Pluto fly-by mission, New Horizons, has a Long-Range Reconnaissance Imager (LORRI) which is also of a Ritchey–Chrétien optical design, with a 208 mm diameter, f/1.8 primary mirror and an effective focal length of 2.63 m (f/12.6). The instrument's mirrors are formed from silicon carbide and it uses three fused silica correcting lenses to produce a flat image plane. Its field of view is 0.29° and its resolution is 1"/pixel over a 350–850 nm range (equal to 60 m on Pluto at its closest approach). The detector is a 1024 × 1024 pixel CCD array rear illuminated and thinned and operated in a frame-transfer mode (Section 1.4.1.2). The planned Lucy mission to Jupiter's Trojan asteroids will carry an updated version of LORRI, called L'LORRI.

A 150 mm, f/3.75 Ritchey–Chrétien is currently operating as the first robotic lunar telescope. Whilst its targets are deep space objects, it is included here as a possible forerunner of lunar-based instruments that are likely to be investigating solar system objects at some time in the future. The lunar-based ultraviolet telescope (LUT) is on board the Chinese National Space Administration's (CNSA) Chang'e 3 lunar lander. The LUT is fixed in position on the lunar lander and is fed by a flat mirror† that tilts in two dimensions to acquire the desired targets. A small flat mirror at 45° to the optical axis and placed just in front of the primary mirror reflects the radiation out to a focus at the side of the instrument (an arrangement known as the Nasmyth focus for terrestrial telescopes). Its field of view is 1.36°. The LUT observes over the 245–320 nm waveband using a 1024 × 1024 pixel CCD detector, illuminated from its back and with enhanced UV sensitivity. The advantage of using a lunar-based telescope lies principally in the long periods of continuous

* The relative velocity of Giotto to Halley's comet during the fly-by was 68 km s⁻¹, so a 1 mm³ particle would hit with an energy of ~2.5 kJ – about the same energy as a rifle bullet.

† Termed a siderostat or coelostat for similar Earth-based systems.

observations of a target that are permitted by the Moon's slow rotation – up to 250–300 hours are possible. The Moon also provides a stable base, allowing high pointing accuracy without the need to consume much power or thruster fuel, as would be needed for a spacecraft-based instrument.

The Cassini Saturn orbiter spacecraft carried two cameras – a narrow angle (i.e. high resolution), 2 m focal length, $f/10.5$, Ritchey–Chrétien reflector (narrow angle camera [NAC]) and a wide angle, 200 mm focal length, $f/3.5$ refractor (wide angle camera [WAC]). Details of the latter are discussed below. The NAC had a field of view of 0.35° square and a resolution of about $1.3''$ per pixel (Figure 1.2). Its mirrors were composed of fused silica while the (refractive) field correctors and the detector entrance window were made from fused silica or calcium fluoride. The instrument had two filter wheels with a design derived from the Hubble Space Telescope's (HST) Wide Field Planetary Camera (WFPC)*. There were a total of 24 filters covering the range 200 nm to $1.05 \mu\text{m}$ with 12 filters in each wheel. Exposures were made using a focal-plane shutter similar to those used for both the Voyager and Galileo missions (the same design of shutter is also used for the WAC). The detector was a 1024×1024 CCD array.

The Mercury orbiter, MESSENGER, carried a 24 mm, $f/22$ off-axis Ritchey–Chrétien NAC (see also Section 1.2.2.1) with a field of view of 1.5° . The instrument was constructed from aluminium with gold coatings for the mirrors and used a 1024×1024 pixel frame transfer CCD detector. It observed over the 700–800 nm wavelength range and its filters rejected thermal radiation at longer wavelengths in order to minimise the heat entering the instrument. At the spacecraft's lowest perihelion,† its ground resolution could be as good as 2 m.

While most detailed observations of solar system objects come from spacecraft physically close to those objects, some terrestrial telescopes can still make contributions. Thus the Keck and Gemini telescopes – all of Ritchey–Chrétien design – have recently been able to track Io's active volcanoes over periods of several years. Operating in the NIR, they use adaptive optics (reference A.1.1) to sharpen the blurring caused by Earth's atmosphere until they can resolve down to a tenth of a second of arc – a linear distance of ~ 300 to ~ 400 km on the surface of Io.

1.2.1.4 Catadioptric Systems

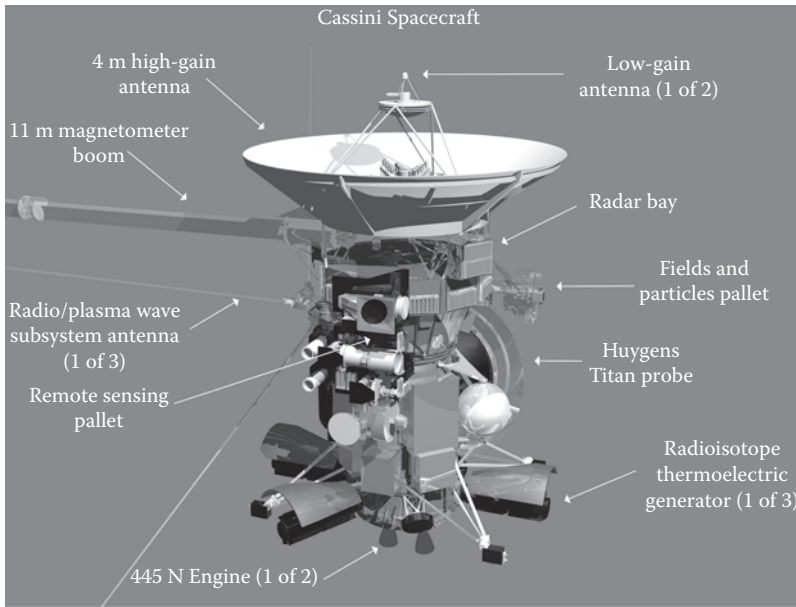
The Super Resolution Camera (SRC – Figure 1.3) on the Mars Express Orbiter uses the Makzutov variation on the Cassegrain design. This has a full-aperture correcting lens which has the secondary mirror aluminised on its centre. The camera has a 90 mm aperture and a 970 mm effective focal length. The instrument uses a 1024×1032 CCD (Section 1.2.1.2) array with $9 \mu\text{m}$ pixels. From a height of 250 km its resolution‡ of the Martian surface is 2.3 m.

Also using an all-spherical catadioptric design, although not actually Makzutovs, were the closely similar imagers on the Mariner 10 (Television Photography Experiment [TPE]),

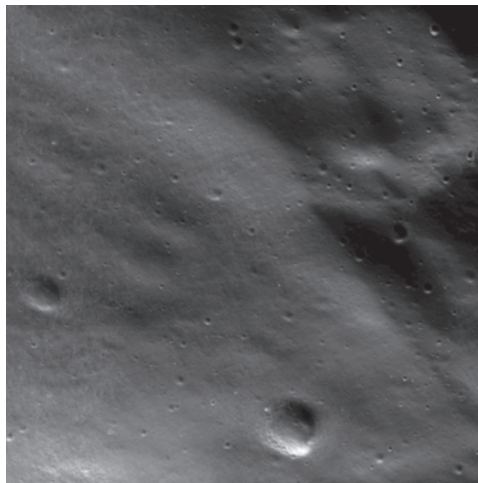
* One of the HST's launch instruments, replaced in 1993.

† The lowest point in its orbit.

‡ Sometimes called the Instantaneous Geometrical Field of View (IGFoV).



(a)



(b)

FIGURE 1.2 (a) The Cassini spacecraft showing the high-resolution Ritchey–Chrétien camera which is the light-coloured tube just left of centre; the WAC (see Section 1.2.2) is just below it. (Courtesy of NASA/JPL-Caltech.) (b) A raw, NAC, Cassini image of part of Iapetus. The large crater at the bottom of the image is about 1.4 km in diameter. (Courtesy of NASA/JPL.)

Voyager 1 and 2 (their NACs) and Galileo spacecraft. In fact, the instrument on Galileo was a modified flight spare from Voyager. The Solid State Imager (SSI) on NASA’s Galileo Jupiter orbiter had a 250 mm diameter $f/3.5$ primary mirror and an effective focal length of 1500 mm ($f/8.5$). There were two full-aperture correcting lenses placed inside the primary

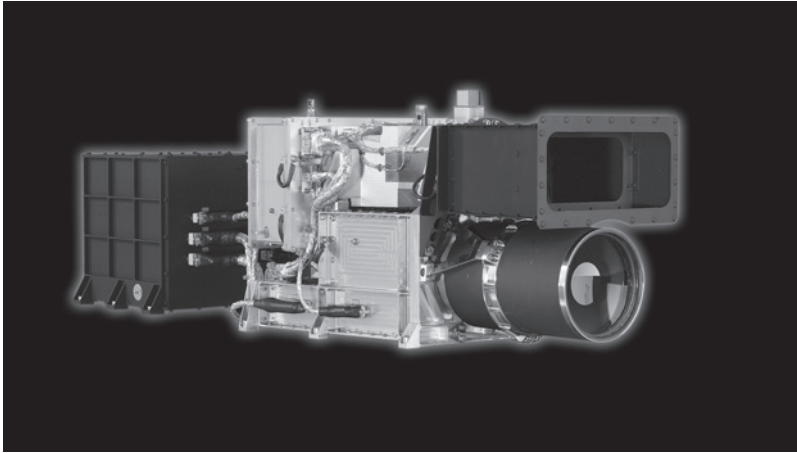


FIGURE 1.3 The Super Resolution Camera of the Mars Express Orbiter spacecraft. The correcting lens with the secondary mirror aluminised on its inner surface can clearly be seen as the lower half of the instrument. The High Resolution Stereo Camera (HRSC) forms the upper half of the instrument and its aperture is above the Makzutov barrel – see Section 1.2.2.1. (Courtesy of Deutsches Zentrum für Luft und Raumfahrt (DLR)/ESA.)

focal point with the secondary mirror attached to the centre of the innermost lens surface. Two further small correcting lenses were placed just before the final focus. The instrument had a 0.46° field of view and eight filters which covered the spectral band from 375 nm to 1.1 μm . Galileo was one of the first spacecraft to use a CCD array as its detector. The CCD had 800×800 pixels and was front illuminated. It was of the buried channel design and used a single set of electrodes (virtual phase CCD – Section 1.4.1.2) with a resolution of $2''/\text{pixel}$.

The Kepler mission's primary aim is the detection of exoplanets (Appendix A, reference A.1.3). However, it was also used to observe Rosetta's comet (67P/Churyumov-Gerasimenko) during a period when it was invisible to terrestrial telescopes. Kepler uses an $f/0.95$ Schmidt camera system with a 1.4 m primary mirror. A mosaic of forty-two 1024×2000 pixel CCDs acts as its detector. Its field of view is thus some 12° across.

Although neither remotely nor robotically operated, the Far Ultraviolet Camera/Spectrograph (FUVCS) (Figure 1.4) used by the Apollo 16 astronauts on the lunar surface is sufficiently similar to the other cameras discussed here to be worthy of inclusion. The Apollo 16 mission to the Moon included a 75 mm, $f/1.0$ Schmidt camera that could obtain images over the 105–155 nm spectral region (and also spectra over the 50–135 nm region by rotating the camera through 90° to point to a reflective diffraction grating and collimator – see Section 1.3). The camera was mounted on a tripod and deployed onto the lunar surface in the landing module's shadow in order to help keep it cool and to reduce solar glare. It was used to observe UV radiation from Earth's upper atmosphere and aurorae as well as from stars and galaxies.

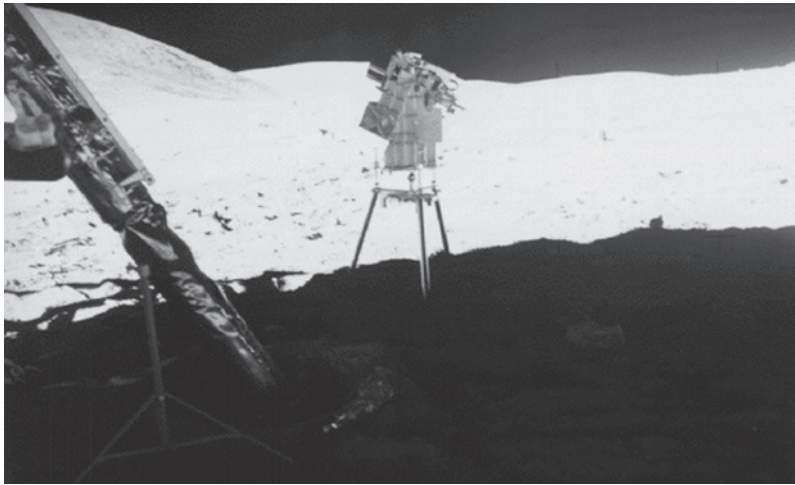


FIGURE 1.4 The Apollo 16 far ultraviolet camera/spectrograph. (Courtesy of NASA.)

The instrument had two correcting lenses – one composed from lithium fluoride which transmitted down to a wavelength of 105 nm thus allowing the Lyman- α line* at 121.6 nm through. The second lens was made from calcium fluoride with a cut-off at 123 nm and so excluded Ly- α emissions. For detecting the shortest wavelengths (in the spectroscopic mode) the corrector lenses were removed. The spherical primary mirror had a reflective coating of rhenium (which has a much higher short wave UV reflectivity than aluminium) and the field of view was 20°.

From a modern perspective, the far UV camera's detector was a rather Heath Robinson system called an electronographic tube (see also Section 1.4.3.5.3). This had a potassium bromide photocathode coated onto a supporting plate curved to match the curved image surface of the mirror and placed at the focal surface. Potassium bromide's electron emission cut-off is at 155 nm, so the system did not respond to the much more plentiful longer wavelength photons. Electrons emitted by the photocathode were accelerated by a –25 kV electrostatic field and magnetically focussed to pass through a central hole in the primary mirror. Most of the electrons then passed through a thin (7.7 nm) plastic membrane at the electron image plane and were absorbed by nuclear grade photographic emulsion (Section 1.4.3.5.3). The emulsion was coated (like conventional photographic film) onto a plastic tape which was pressed against the membrane during an exposure and then moved on for the next exposure. After alignment of the instrument onto a desired target by an astronaut the exposures were obtained automatically. The film cassette was brought back to Earth by the astronauts for processing.

The backup camera to the one used during the Apollo 16 mission was used in a slightly adapted form during the Skylab-4 mission to obtain UV images of comet Kohoutek.

* A spectrum line arising from electron transitions between the first and second energy levels in the hydrogen atom – see Section 1.3.3.

1.2.1.5 Gregorian Systems

Several solar spacecraft, such as Hinode, which observed the 2012 transit of Venus, have carried Gregorian-type cameras. The Solar Optical Telescope (SOT) on board Hinode has a 0.5 m aperture and 0.2" resolution over a 0.11° square field of view. Stratoscope 2,* a balloon-borne telescope that flew missions between 1963 and 1971 to study, amongst other topics, planetary atmospheres at infrared wavelengths, was a 0.91 m variant on a Gregorian telescope. The primary, fused silica mirror operated at f/4 and the secondary converted this to f/33. A flat mirror set at 45°, just before the primary mirror, reflected the light beam sideways into the optical train of the detector and the guidance system. The camera operated over the visible and NIR range using photography initially and later TV cameras.

1.2.1.6 Custom-Designed Systems

The Mars Odyssey Orbiter carries a Thermal Emission Imaging System (THEMIS) that covers the range 425 nm to 14.88 µm and provides mainly mineralogical information about Mars. The anastigmatic† instrument is based upon three aspherical off-axis mirrors feeding separate infrared and visual detector arrays via a beam splitter. The mirrors are diamond-turned from aluminium blocks and subsequently polished and nickel plated. THEMIS has an effective focal length of 200 mm at f/1.6 (aperture 120 mm). The field of view is 3.5° × 4.6° and its resolution at the Martian surface is 18 m/pixel (visual) and 100 m/pixel (infrared). Ground truth data (Section 7.2.7) to calibrate its measurements have been provided by Opportunity's Miniature Thermal Emission Spectrometer (MiniTES – Sections 7.2.1 and 7.2.2.1).

Nine filters cover the spectral region from 6.78 to 14.88 µm. The thermal radiation is detected by an uncooled 240 × 320 pixel microbolometer array (Section 1.4). The filters are in the form of strips, each covering a line 16 pixels wide, and the images are built up by pushbroom scanning as the spacecraft's orbital motion sweeps the field of view over the Martian surface. The signals from the detectors are read out by TDI (see Section 1.4.1.2) to fit in with the scanning method. Five filters in the forms of 192-pixel wide strips are used to cover the visible and NIR and their images are obtained by a 1024 × 1024 pixel frame scan CCD giving a 2.6° field of view (Figure 1.5).

Rosetta's Optical, Spectroscopic and Infrared Remote Imaging System (OSIRIS) NAC was also based upon a three-mirror anastigmatic design. The mirrors were formed from silicon carbide with the primary and secondary mirrors having aspherical surfaces whilst the tertiary was spherical. The instrument had an effective focal length of 717 mm, a 90 mm aperture, a 2.2° field of view and an angular resolution of 3.8" – corresponding to a surface resolution of about 20 mm at best. It used an UV-enhanced 2048 × 2048 pixel CCD array and covered the 250 nm to 1 µm spectral range with 12 wide to medium band filters.

The f/5.6 WAC within the OSIRIS package had a 12° field of view provided by two aspherical off-axis mirrors. Its focal length was 130 mm and its angular resolution 20". Its 14 narrow band filters covered from 250 to 630 nm and its detector was a 2048 × 2048 pixel CCD.

* Operated by NASA, the Office of Naval Research (ONR) and the Naval Research Laboratory (NRL).

† An optical system in which both astigmatism and field curvature are corrected. See reference A.1.1 for a detailed discussion of the Seidel aberrations of optical systems, or other sources listed in Appendix A.

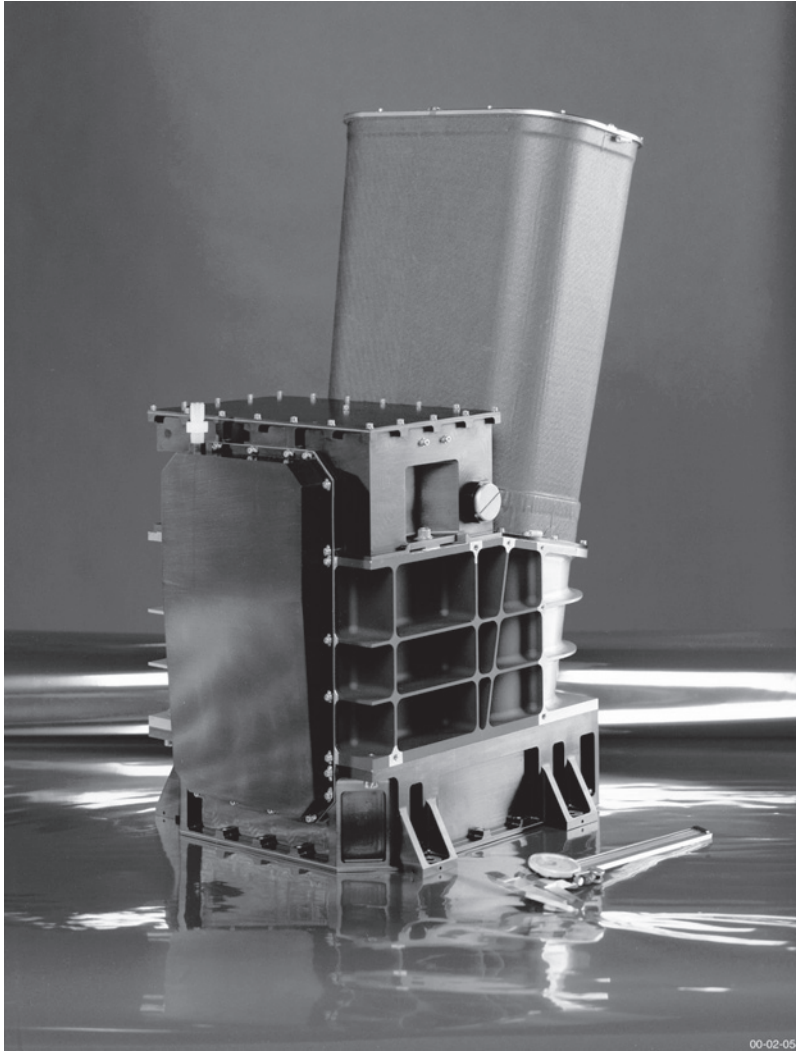


FIGURE 1.5 Mars Odyssey's THEMIS camera. The entrance aperture is at the top of the smooth rectangular tube that slants slightly to the right. (Courtesy of NASA/JPL-Caltech/Arizona State University.)

Another custom-designed reflective camera is Ralph on board the New Horizons spacecraft. Ralph operates over the 400–975 nm region (visible and NIR) and can obtain both direct images and spectra (Section 1.3). Its design is anastigmatic with three aspherical, off-axis mirrors. The primary mirror has a concave elliptical shape and a 75 mm aperture. The secondary mirror is a convex hyperbola and the tertiary mirror is a concave ellipse. The final focal length is 658 mm and the field of view 5.7° by 1.0°. A dichroic* beam splitter sends radiation over the range 400 nm to 1.1 μm to the imager and the longer wave radiation to the spectrograph.

* A mirror with a coating that reflects at some wavelengths and is transparent at others. For example, a thin gold coating reflects at 90% or better for wavelengths longer than 600 nm and is transparent for wavelengths shorter than 450 nm.

Images are obtained as the spin of the spacecraft scans the field of view over the target. The detectors are six 32×5024 CCD arrays operated in TDI mode (Section 1.4.1.2). Two of the arrays produce panchromatic images over the 400–975 nm range. The other four obtain images through blue, red and infrared filters and a narrow band methane filter centred on 885 nm (see also JunoCam below). There are also two wide band filters, one of which acts as a backup to the main navigation instrument (LORRI – see above). A seventh 128×5024 pixel CCD operating in frame transfer mode (Section 1.4.1.2) aids the spacecraft's navigation.

The mirrors for Ralph were formed by computer-controlled diamond turning of aluminium blocks with special processing to reduce the surface roughness and grooving normally left by the process – giving their surfaces a roughness of about 6 nm. To achieve the Rayleigh limit of resolution, α ,

$$\alpha = \frac{1.220\lambda}{d} \text{ radians} \quad (1.12)$$

(where d is the aperture diameter) of an optical system requires a surface accuracy for the mirrors in the region of $\lambda/8$ – which at 400 nm would be about 50 nm. So, neither any additional polishing of the mirror surfaces nor separate reflective coatings were needed.

The ExoMars Trace Gas Orbiter* has Colour and Stereo Surface Imaging System (CaSSIS) on board to look for sources of trace gases and to investigate surface processes – such as erosion, sublimation and volcanism – as possible contributors of gases to the atmosphere. Its telescope is a three-mirror anastigmat with a 135 mm aperture and an 880 mm focal length. Its field of view is 0.88° by 1.34° and its angular resolution is $1'$ per pixel. The detector is a 2024×2024 CMOS array (Section 1.4.1.3). It has filters enabling images to be obtained in the wavelength ranges 400–550 nm, 525–775 nm, 790–910 nm and 875 nm– $1.025 \mu\text{m}$.

The Earth resources spacecraft, Landsat-7, carries the Enhanced Thematic Mapper plus (ETM+) in which a scanning mirror feeds a collimator based upon a Ritchey–Chrétien design followed by two correcting mirrors focussing at the primary focus (for the visible and NIR bands) with some of the radiation redirected through a relay system to a secondary, cold, focus (for the MIR bands).

Three identical three-mirror off-axis aspherical anastigmatic telescopes are carried by the Proba-V spacecraft. They each have fields of view of 34° and are angled to each other to give a total coverage of 102° – providing an observed swath 2285 km across at Earth's surface. Their effective focal lengths are 110 mm and best ground resolutions 100 m. They have four filters each and operate over the 462 nm to $1.6 \mu\text{m}$ spectral range in order to survey vegetation on Earth. The long wave filter uses a separate light path through the telescope and is diverted by a 45° mirror to a separate detector. Three linear 6000 pixel CCD (Section 1.2.1.2) detectors are used for the shorter wavelengths and three staggered linear 1024 pixel InGaAs photodiode detectors (Section 1.4.1.4) for the long wavelength band.

* ESA/RKA. RKA – Federal'noye kosmicheskoye agentstvo Rossii (Russian Federal Space Agency).

1.2.2 Refracting Cameras

Today's space cameras based upon lenses are either mostly similar to the basic astronomical refracting telescope with a single objective lens (usually achromatised for its operating wavelengths – Figure 1.1e) projecting its images directly onto the detector instead of into an eyepiece or more like a high-quality digital commercial single lens reflex (SLR) camera as sold to the general public. Their detector arrays are usually CCDs or other solid state detector arrays.

1.2.2.1 Telescope-Type Systems

In the early days of space exploration, photographic cine cameras and vidicon TV cameras were used (Section 1.4.3.5). Indeed, the very first images obtained from space – of parts of Earth – used an off-the-shelf 35 mm cine camera. The camera was launched to a height of 105 km in October 1946 by an ex-World War II German V2 rocket and its main modifications were firstly a reinforced film cassette so that it could survive the $150 \text{ m}\cdot\text{s}^{-1}$ impact when the rocket fell back to Earth and secondly slowing the frame rate to one frame every second and a half.

Film photography was used by several of the Moon-fly-by/Earth-return Zond spacecraft since their returns to Earth meant that the film could be retrieved. Zond-5 was the first such successful mission although, due to a fault, only images of Earth were obtained. Zond-7 carried a 300 mm focal-length camera and obtained $56 \text{ mm} \times 56 \text{ mm}$ colour and panchromatic images. Zonds 6 and 8 both used 400-mm-focal-length cameras and their isopanchromatic images were $130 \text{ mm} \times 180 \text{ mm}$ in size. Zond-6 however crash landed and only one image was retrieved.

The lunar impactor, Ranger 7, used six slow-scan vidicon cameras – two WACs and four NACs—to obtain the first close-up images of the Moon's surface. The WACs used 25 mm focal length lenses and had fields of view of 25° , while the NACs used 76 mm focal length lenses and had 8.5° fields of view. The vidicon detector windows were coated with an antimony-sulphide/oxy-sulphide sensitive layer and scanned 1150 lines in 2.5 seconds or 300 lines in 0.2 seconds. Over 4000 images were obtained in the last 14 minutes before the spacecraft hit the Moon's surface at $2.6 \text{ km}\cdot\text{s}^{-1}$.

The Dawn spacecraft, which is currently orbiting Ceres* having previously visited Vesta, carries two refracting telescopes for imaging and to aid navigation when close to its targets. The telescopes, called the framing cameras (FCs), are identical and each is a complete instrument in its own right. They are physically separate and having two of them provides for backup in case one of them fails. The objective lens has a 20 mm aperture and a 150 mm focal length ($f/7.5$) and is essentially an achromatic triplet. The elements of the triplet though are widely separated and the third element is split into two (i.e. there are a total of four lenses in the system). The first element is a crown glass converging lens with an aspherical front surface to compensate for spherical aberration. It is followed by two flint glass diverging lenses and the final element, also of flint glass, is again a converging

* A possible visit by Dawn to asteroid 145 Adeona has been abandoned in favour of continuing observations of Ceres during its perihelion passage.

lens. The focal position is maintained to within $\pm 15 \mu\text{m}$ over a wide temperature range by mounting the two central lenses separately in a tube with a different thermal expansion coefficient from the rest of the camera. The cameras have 5.5° square fields of view and operate from 400 nm to $1.05 \mu\text{m}$ using one of the eight available filters (one broad band, the others all narrow band). The detectors are 1024×1024 CCDs with a best resolution of 17 m/pixel at Vesta and 66 m/pixel at Ceres.

The Mercury fly-by and orbiter spacecraft, MESSENGER, carried a reflective NAC and a refractive WAC. The WAC used two biconvex converging lenses and two biconcave diverging lenses in two groups separated by about 20 mm. Its focal length was 78 mm and its aperture 7 mm. It used 12 filters and operated over the 395 nm to $1.04 \mu\text{m}$ spectral range. The detector was a 1024×1024 CCD array giving a resolution of $36''$ – corresponding to about 20 m on Mercury's surface at perihelion. In 2014, it showed the presence of water ice in permanently shadowed craters at Mercury's North Pole.

As mentioned above, the Cassini spacecraft carried a WAC with refracting optics (Figure 1.2). The lenses were spares originally manufactured for the Voyager missions. The camera was $f/3.5$ with a focal length of 200 mm and a 3.5° square field of view, giving a resolution of $13''/\text{pixel}$. The lenses were fabricated from radiation-hardened glass or lithium fluoride. It had two filter wheels, each carrying nine filters enabling images over the 380 nm to $1.05 \mu\text{m}$ region to be obtained. The detector was a 1024×1024 CCD array.

The Eros orbiter, NEAR Shoemaker, carried a 50 mm, $f/3.4$ refractor as its imaging instrument. The camera, called the Multi-Spectral Imaging system (MSI), used a five-element lens and had a $2.3^\circ \times 2.9^\circ$ field of view. It used one wide band and seven narrow band filters, covering the spectral range from 400 nm to $1.1 \mu\text{m}$, chosen to facilitate the identification of silicate minerals containing iron. The detector was a 244×537 pixel CCD array that was operated at the ambient temperature (typically -30°C to -40°C) with a best resolution of $20''/\text{pixel}$. From NEAR Shoemaker minimum height before landing of 120 m, this resolution corresponds to a distance of about 10 mm on the surface of Eros.

1.2.2.2 Camera-Type Systems

Examples of the 'commercial digital SLR' type of camera are to be found widely. Thus, JunoCam on the Juno spacecraft uses a 14-element lens. Its focal length is 11 mm and it has a field of view of 58° . The lens' T/number* is 3.2. A 1200×1600 pixel CCD is used as the detector and this has a field of view of 3.4° by 18° . The point of view is scanned across the planet by the spacecraft's rotation to build up the full image with TDI (Section 1.4.1.2) read-out. It is designed to obtain colour images of Jupiter with a best resolution of 3 km per pixel (a nearly 40 times improvement of the best Jovian images obtained by the HST†). Colour filters in the form of strips and covering the visible region and into the NIR are bonded to the detector

* A similar measure to a lens' f/number or focal ratio, but including the effects of absorption within the elements of the lens.

† The HST has a yearly programme (Outer Planet Atmospheres Legacy [OPAL]) of obtaining global maps of all the outer planets.

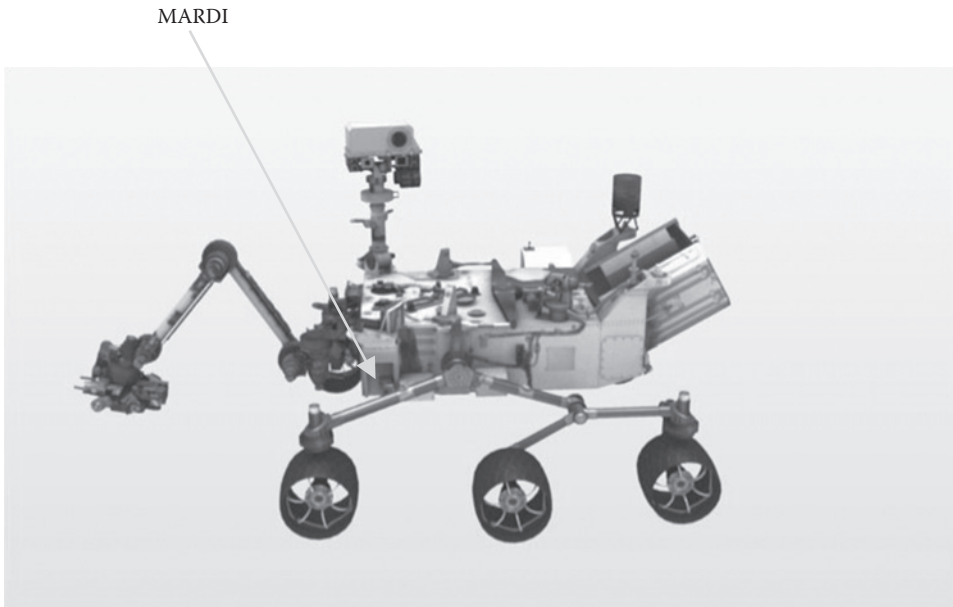


FIGURE 1.6 MARDI mounted on the Curiosity rover. (Courtesy of NASA/JPL-Caltech.)

and are pushbroom scanned across the planet by the spacecraft's rotation. Additionally, there is a narrow band filter centred on the methane absorption line at 889 nm.

JunoCam is a development of the Mars Descent Imager camera (MARDI) mounted on the Mars Science Laboratory's (MSL) Martian rover, Curiosity (Figure 1.6). The main changes from that instrument are radiation hardening (including making the first five elements of the lens from radiation-proof glass) and a 6 mm thick titanium housing. MARDI also used a Bayer* arrangement of filters similar to those used in most publically available digital cameras to generate its colour images.

The Lunar Orbiter/Asteroid fly-by mission, Clementine (see also Section 1.2.1.2), had several cameras. The UV and Visible camera covered from 250 nm to 1 μm and had five narrow band filters and one broadband filter. It used fused $f/1.96$ silica lenses with an aperture of 46 mm. The detector was a 288×384 pixel CCD array. Its field of view was $4.2^\circ \times 5.6^\circ$ and its lunar surface resolution was between 100 and 325 m. The NIR camera operated between 1.1 and 2.8 μm with six filters and a 256×256 pixel InSb photovoltaic detector array (Section 1.4.1.4). Its $f/3.3$ lens had a focal length of 96 mm giving it surface resolution between 150 and 500 m.

In addition to Mars Express' SRC, Figure 1.3 shows the HRSC. This is a seven-element apochromatic† lens with a flat image plane and very little distortion. This is a lens design that is often used for high-quality consumer telephoto lenses. It has a 31 mm aperture and

* For each set of four pixels, two have green filters, one a red filter and one a blue filter.

† An optical system in which chromatic aberration (different focal lengths for different colours) has been corrected at three different wavelengths. See reference A.1.1 for a detailed discussion of the aberrations of optical systems, or other sources listed in Appendix A.

a 175 mm focal length ($f/5.6$). Five filters (blue, green, red, NIR and semi-panchromatic) enable it to image over the 400 nm to 1 μm region. The detector is a CCD (Section 1.2.1.2) of somewhat unusual configuration – it has nine lines, one for each channel and each 1×5184 pixels in size (cf. Ralph, above). Stereo images are produced by observing the same region three times over as the spacecraft moves around its orbit using forward-facing, nadir-facing and backward-facing sensors. Its resolution of the Martian surface is about 10 m. The HRSC was originally built as a duplicate instrument for the RKA's Mars 96 mission (destroyed during its launch in 1996).

The Indian Space Research Organisation's (ISRO) Mars Orbiter Mission (MOM) uses a commercial, off-the-shelf, 105 mm focal length, $f/4.0$ telephoto lens (Mars Colour Camera – MCC). It has a field of view of 8.8° and a surface resolution varying from 15 m (when at periareon – 420 km above the Martian surface) to 4 km (when at apareon – 70,000 km above the Martian surface). The detector is a 2048×2048 CCD array using Bayer-pattern filters operating over the 400–700 nm spectral range. The failed Mars lander, Schiaparelli's descent camera (DECA), would have obtained monochromatic images of its landing area. The camera had a focal length of 6.65 mm, a field of view of 60° and used a CMOS array (Section 1.4.1.3) as its detector.

The SMART-1* lunar orbiter carried a small camera constructed from off-the-shelf components with a 1024×1024 CCD detector. Asteroid-Moon Micro-Imager Experiment (AMIE) imaged in white light plus through filters at 750, 915 and 960 nm with the filters deposited directly onto the CCD pixels. Its best surface resolution was 27 m and its objective was to look at lunar surface mineralogy.

JAXA's Akatsuki's (also known as Venus Climate Orbiter) 2 μm NIR camera is designed to study the middle to lower part of Venus' atmosphere using windows in the carbon dioxide absorptions at 1.74 and 2.3 μm . It is based upon a triplet lens comprising a zinc sulphide and two quartz elements and has five narrow band filters. Its focal length is 84 mm with a 12° field of view and its angular resolution is 1° . A 1040×1040 pixel platinum silicide array is used as the detector.

The ExoMars Rover mission is planned for a launch in 2020 with a landing on Mars in 2021. The rover will carry three cameras mounted as a single rotatable and tiltable unit, called PanCam, at the top of a mast. The two identical WACs are planned to have fields of view of 32.3° supplied by 22 mm focal length $f/10$ lenses. Each camera will have 11 filters covering the range 400–1050 nm. The detectors are to be 1024×1024 CMOS arrays (Section 1.4.1.3) with an angular resolution of $2'$ per pixel (corresponding to 1.3 mm on the surface at a distance of 2 m). The two WACs will be separated by 500 mm in order to enable stereoscopic images to be obtained and are sighted on the same spot at a distance of about 5 m from the rover.

The Hayabusa-2 asteroid sample and return mission's lander, Mobile Asteroid Surface Scout (MASCOT) carries a lens-based camera designed on the Scheimpflug[†] principle so that its images are in focus from 150 mm to infinity. The Scheimpflug design may be used

* Small Missions for Advanced Research in Technology.

† Theodor Scheimpflug, a captain in the Austrian army, used the principle for aerial photography in the early twentieth century.